© 2020. Published by The Company of Biologists Ltd | Journal of Cell Science (2020) 133, jcs248583. doi:10.1242/jcs.248583

RESEARCH ARTICLE

The spectrin-based membrane skeleton is asymmetric and remodels during neural development in *C. elegans*

Ru Jia[1], Yongping Chai[1], Chao Xie[1], Gai Liu[2], Zhiwen Zhu[1], Kaiyao Huang[2], Wei Li[3,*] and Guangshuo Ou[1,*]

ABSTRACT

Perturbation of spectrin-based membrane mechanics causes hereditary elliptocytosis and spinocerebellar ataxia, but the underlying cellular basis of pathogenesis remains unclear. Here, we introduced conserved disease-associated spectrin mutations into the *Caenorhabditis elegans* genome and studied the contribution of spectrin to neuronal migration and dendrite formation in developing larvae. The loss of spectrin resulted in ectopic actin polymerization outside of the existing front and secondary membrane protrusions, leading to defective neuronal positioning and dendrite morphology in adult animals. Spectrin accumulated in the lateral region and rear of migrating neuroblasts and redistributes from the soma into the newly formed dendrites, indicating that the spectrin-based membrane skeleton is asymmetric and remodels to regulate actin assembly and cell shape during development. We affinity-purified spectrin from *C. elegans* and showed that its binding partner ankyrin functions with spectrin. Asymmetry and remodeling of the membrane skeleton might enable spatiotemporal modulation of membrane mechanics for distinct developmental events.

KEY WORDS: Cell migration, Cytoskeleton, Dendrite formation, Membrane mechanics, Spectrin, Neural development

INTRODUCTION

The development of the nervous system requires the correct positioning of neurons and the accurate sprouting and elongation of neurites, laying the foundation for functional neuronal connectivity. The motility of neuronal cells and the growth cone is initiated by environmental-cue-activated transmembrane receptors and followed by asymmetric actin polymerization in the leading edge and the extension of the front of the cell (Leterrier et al., 2017; Pollard and Cooper, 2009; Tang and Jin, 2018). Despite the wealth of information on the biochemical mechanism of neural development, ranging from the guidance cues and their receptors to the protein machinery that powers motility, the physical regulation of neural development, in particular, the underlying membrane mechanics, is mostly unexplored.

The spectrin-based membrane skeleton is essential for the structural integrity of the plasma membrane and protects cells from mechanical stresses in both erythrocytes and many non-erythrocyte cells (Liem, 2016). The functional unit of spectrin is composed of a rod-shaped tetramer that consists of two antiparallel heterodimers of α-spectrin and β-spectrin (Liem, 2016). Spectrin interacts with the actin cytoskeleton and associated proteins to form a static polygonal lattice structure underneath the plasma membrane. Recent super-resolution imaging studies uncovered that spectrin creates an ordered periodic longitudinal array around the circumference of axons and dendrites (Han et al., 2017; He et al., 2016; Leterrier et al., 2017; Wang et al., 2019; Xu et al., 2013). In addition to mechanical support, the membrane-associated periodic skeleton serves as a dynamic platform for G-protein-coupled receptor and cell adhesion molecule-mediated receptor tyrosine kinase signaling (Zhou et al., 2019). Mutations in human spectrin genes impair spectrin-based membrane mechanics and cause various diseases. For example, the hereditary elliptocytosis (HE)-associated α-spectrin (SPTA1) L260P mutation locks spectrin in the closed dimer conformation and destabilizes the plasma membrane (Gaetani et al., 2008; Harper et al., 2013). The spinocerebellar ataxia type 5 (SCA5)-associated β-III-spectrin (*SPTBN2*) deletion disrupts the spectrin tetramer conformation and alters the localization of synaptosomal proteins in the cerebellum (Ikeda et al., 2006; Ranum et al., 1994). Knockout of β-II-spectrin (*SPTBN1*) in mouse neural progenitors disrupts axonal growth, stability, and synaptic cargo transport (Lorenzo et al., 2019). These studies establish the importance of spectrin in the nervous system and reveal the association between spectrin deficiency and neurodegenerative disorders; however, the function of spectrin-based membrane mechanics in neural development remains unclear.

To model spectrin-associated diseases in animals, we have previously introduced conserved disease-associated mutations into the *Caenorhabditis elegans* α- and β-spectrin genes (*spc-1* and *unc-70*, respectively; Jia et al., 2019). These mutations affect membrane mechanics, and cause uncoordinated animal movement, mimicking the syndromes of the patients. Using these animals, we previously uncovered a novel function of spectrin in cilium formation in nematodes and showed the conserved mechanism in mammals (Jia et al., 2019). Here, we chose the *C. elegans* Q neuroblasts as a tractable experimental system to study the function and behavior of spectrin in developing neural progenitors. The Q neuroblasts, QR on the right side of the animal and QL on the left, undergo an identical pattern of asymmetric cell divisions, directional migration, apoptosis, and neurite growth in the first larval stage (Ou and Vale, 2009; Sulston and Horvitz, 1977). The Q cell descendants move to highly stereotypical positions along the anterior and posterior body axis, but in opposite directions, with QR and progenies (collectively abbreviated as QR.x) migrating anteriorly and QL and progenies (QL.x) migrating posteriorly (Fig. 1A,B). We previously developed fluorescence time-lapse microscopy methods and reporters to study cell polarity and the actin cytoskeleton in migrating Q cells (Feng et al., 2017; Ou and

[1]Tsinghua-Peking Center for Life Sciences, Beijing Frontier Research Center for Biological Structure, McGovern Institute for Brain Research, School of Life Sciences and MOE Key Laboratory for Protein Science, Tsinghua University, Beijing 100084, China. [2]Key Laboratory of Algal Biology, Institute of Hydrobiology, Chinese Academy of Sciences, Wuhan 430072, China. [3]School of Medicine, Tsinghua University, Beijing 100084, China.

*Authors for correspondence (guangshuoou@tsinghua.edu.cn; weili_med@mail.tsinghua.edu.cn)

K.H., 0000-0001-8669-1065; G.O., 0000-0003-1512-7824

Handling Editor: Michael Way
Received 7 May 2020; Accepted 25 June 2020

Journal of Cell Science (2020) 133, jcs248583. doi:10.1242/jcs.248583

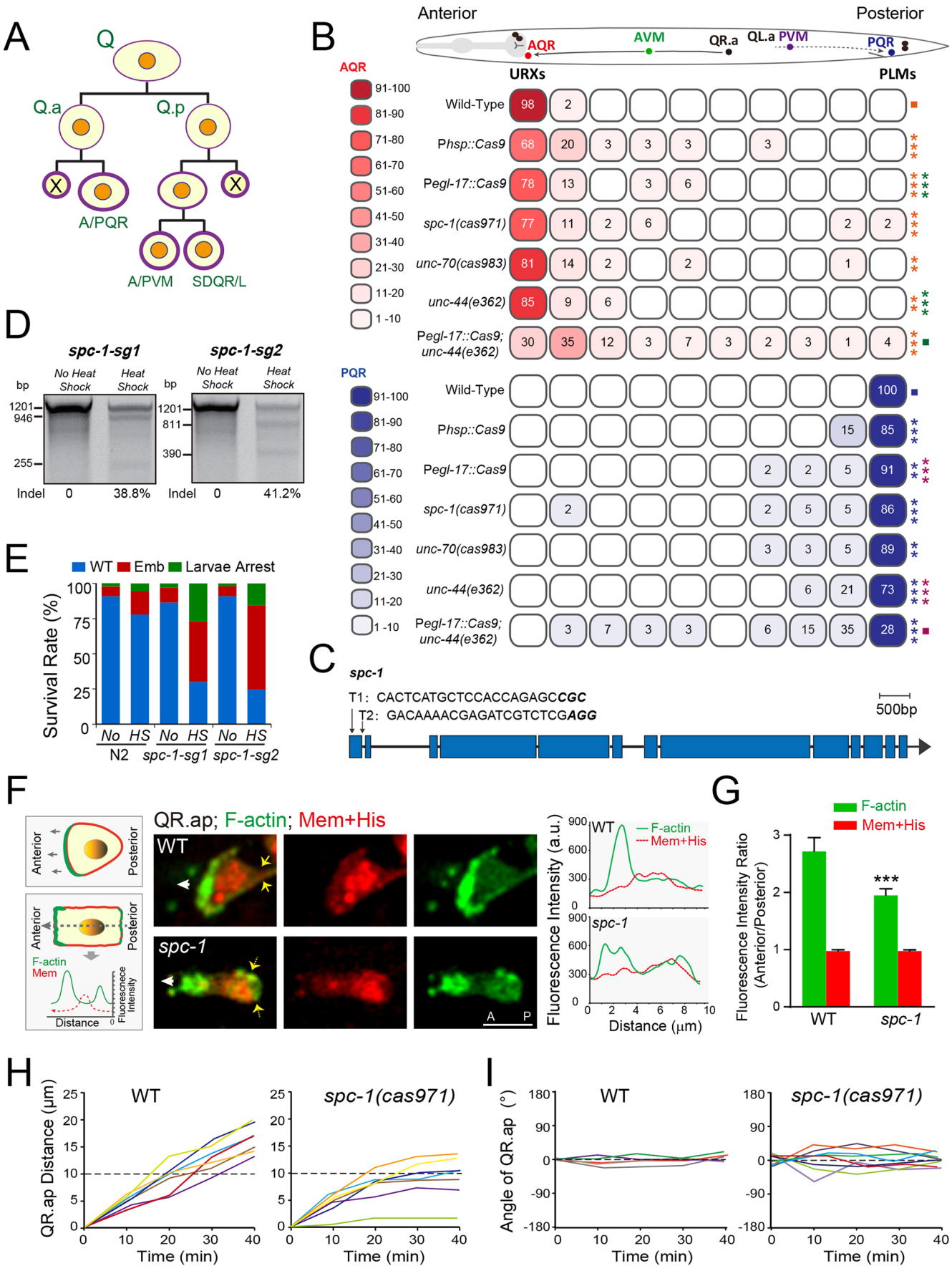

Fig. 1. See next page for legend.

Fig. 1. SPC-1 regulates migration of the *C. elegans* Q neuroblast. (A) Schematic of Q neuroblast lineages. QL and QR neuroblasts divide three times and each generate three neurons (QL: PQR, PVM, and SDQL; QR: AQR, AVM, and SDQR) and two apoptotic cells (X). (B) A color-coded heatmap showing scoring of the position of AQR and PQR neurons in L4-stage animals of the indicated genotypes. As indicated in the schematic overview of Q cell migration at the top, the QR descendant AQR migrates anteriorly, and the QL descendant PQR migrates posteriorly. The full length between the URX neurons and the tail (PLM) is divided into ten blocks, and the percentage of AQRs or PQRs that stopped within each block are listed. The color (red for AQR and blue for PQR) intensity of the blocks symbolizes the range of percentage values. n>50 for all genotypes. Statistical significance compared to the control (■) with matching color code is based on χ^2 tests, **P<0.001, ***P<0.001. (C) Schematic of *spc-1* gene model and sgRNA sequences. Both sg1 (T1) and sg2 (T2) target the first exon. (D) Representative gels of the T7EI assay for *spc-1* PCR products amplified from the genomic DNA of worms expressing P*hsp::Cas9* and P*U6::spc-1-sg1* (left) or P*U6::spc-1-sg2* (right) with or without heat-shock treatment. Percentage of DNA with insertion and deletion is indicated. (E) Quantification of embryo survival rates in WT and *spc-1* conditional knockouts. n=50–100 animals from three generations. No, no heat shock; HS, heat shock. (F) Left: schematic diagram of fluorescence imaging and line scan quantification. Middle: fluorescence images of GFP-labeled F-actin (green) with mCherry-labeled plasma membrane and histone (Mem+His, red) in QR.ap cells in WT and *spc-1(cas971)* animals. Yellow arrows show the rear of migrating cells; white arrows indicate the direction of migration. A and P indicate the anterior–posterior orientation. Scale bar: 5 µm. Right: line scans (performed as in the left panel) of fluorescence intensities across the representative migrating cells shown in the middle panel. (G) F-actin (green) fluorescence intensity ratio of the anterior and to the posterior, the corresponding mCherry membrane intensity ratio was used as an internal control. See Fig. 2A (dashed line) for details of how the anterior and the posterior regions were defined. Data are mean±s.e.m. of n=10 cells. Statistical significance is based on Student's t-test, ***P<0.001. (H,I) Quantification of the QR.ap migration distance (H), and angle (I). Each line represents the measurement from one time-lapse movie of migration of a QR.ap cell.

Vale, 2009; Tian et al., 2015; Wang et al., 2013; Zhu et al., 2016). Using this system, we show that spectrin is crucial for neuronal migration and dendrite formation, and that the spectrin-based membrane skeleton is asymmetrically assembled and remodels in developing neuroblasts.

RESULTS

Spectrin regulates neuronal migration by preventing ectopic actin assembly

The germline deletion of α-spectrin (*spc-1*) or β-spectrin (*unc-70*) leads to embryonic lethality (Hammarlund et al., 2000; Norman and Moerman, 2002). To study the function of spectrin in postembryonic neural development, we generated weak loss-of-function alleles or conditional mutations of spectrin. Our previous study introduced the disease-associated α-spectrin L260P variation or β-III–spectrin in-frame deletion into the *C. elegans spc-1(cas971)* or *unc-70(cas983)* locus, respectively (Jia et al., 2019). Both alleles produced viable progenies, allowing the dissection of the role of spectrin in neural development. As a complementary approach, we used the somatic CRISPR-Cas9 method (Shen et al., 2014) in which the Cas9 endonuclease is expressed under the control of the Q cell-specific promoter P*egl-17* or the heat-shock gene *hsp-16.2* promoter P*hsp* to create conditional mutants of *spc-1* within Q cell lineages or during Q cell development. T7 endonuclease I (T7EI)-based assays demonstrated that these transgenic animals produced molecular lesions with the expected sizes at the target loci of *spc-1* after heat-shock induction of Cas9 expression (Fig. 1C,D). In line with the reported phenotypes of the *spc-1(cas971)* animals (Jia et al., 2019), the *spc-1* conditional mutant embryos, but not wild-type (WT) embryos, exhibited embryonic lethality and larval arrest (Fig. 1E), demonstrating the success in producing conditional mutations in the *spc-1* locus. In these animals, we examined the final positions of the QR and QL descendants QR.ap and QL.ap, which become the AQR and PQR neurons after long-distance migration towards the anterior or posterior, respectively. Compared with the positions in WT animals, AQR localized at a more posterior position, and PQR was confined to a more anterior region in *spc-1(cas971)* or *unc-70(cas983)* or in somatic CRISPR-Cas9-created *spc-1* conditional mutants, indicating an essential role of spectrin in cell migration (Fig. 1B; Fig. S1A). The cell migration defects of Q-cell specific *spc-1* mutants suggested a cell-autonomous contribution of spectrin to cell migration.

To understand the cellular mechanism by which cell migration is reduced in *spc-1* mutants, we performed fluorescence time-lapse analysis of cell morphology and the actin cytoskeleton in migrating Q.ap cells (Ou and Vale, 2009). We labeled the plasma membrane and nucleus using mCherry tagged with a myristoylation signal and a histone, and the actin cytoskeleton using GFP-tagged with the actin-binding domain of moesin (GFP::moesin ABD). In WT animals, AQR extends a large lamellipodium and forms a fan-like morphology (Fig. 1F; Fig. S1B). Strikingly, the morphology of the *spc-1*-mutant AQR was perturbed, including the formation of a square-shaped cell without a persistent anterior–posterior polarity during migration (Fig. 1F; Fig. S1B). In WT migrating AQR cells, GFP::moesin ABD-marked F-actin accumulates in the leading edge but is absent from the lateral region and the rear. The *spc-1*-mutant AQR cell contains GFP::moesin ABD fluorescence in the leading edge (i.e. anterior); however, ectopic GFP fluorescence is detectable in the lateral region and the rear (i.e. posterior), resulting in an even distribution of F-actin along the entire plasma membrane (Fig. 1F). The fluorescence intensity ratio between the anterior and the posterior was reduced from 2.7-fold in WT to 1.9-fold in *spc-1* mutant AQR cells (Fig. 1G), indicating a defective organization of the actin cytoskeleton. In agreement with the final reduction of AQR migration in adult animals, AQR failed to persistently extend the lamellipodium and translocate the cell body towards the anterior, reducing the migration distance and persistent polarity over time (Fig. 1H,I). These results show that spectrin is essential for F-actin organization during cell migration. Given the abnormal actin assembly away from the front of the cell, we postulate that spectrin-based membrane mechanics might act in the posterior to inhibit ectopic actin polymerization.

Asymmetric distribution of the membrane skeleton in migrating neuroblasts

To visualize the cellular distribution of endogenous spectrin proteins during cell migration, we constructed knock-in (KI) animals to mark SPC-1 and UNC-70 with GFP (Jia et al., 2019). We genetically crossed the GFP–spectrin KI markers into a transgenic animal that expressed mCherry plasma membrane and histone reporters within Q cell lineages. GFP-tagged SPC-1 or UNC-70 was absent from the leading edge but accumulated in the posterior of the migrating Q.a, Q.p, Q.ap, and Q.pa cells (Fig. 2A–E; Fig. S1C). Quantification of the fluorescence intensity ratio between the front and the posterior (indicated by dashed lines in Fig. 2C,D) showed that GFP–spectrin in the posterior was ∼2.7–2.9-fold brighter than that in the anterior (Fig. 2A–E; Fig. S1C). In both the QL and QR lineages, GFP::SPC-1 or UNC-70::GFP showed a similar enrichment in the posterior of migrating cells (Fig. 2C,D; Movies 1, 2). We did not detect any change in red fluorescence of the mCherry-tagged plasma membrane and histone throughout Q cell development (Fig. 2E;

Journal of Cell Science (2020) 133, jcs248583. doi:10.1242/jcs.248583

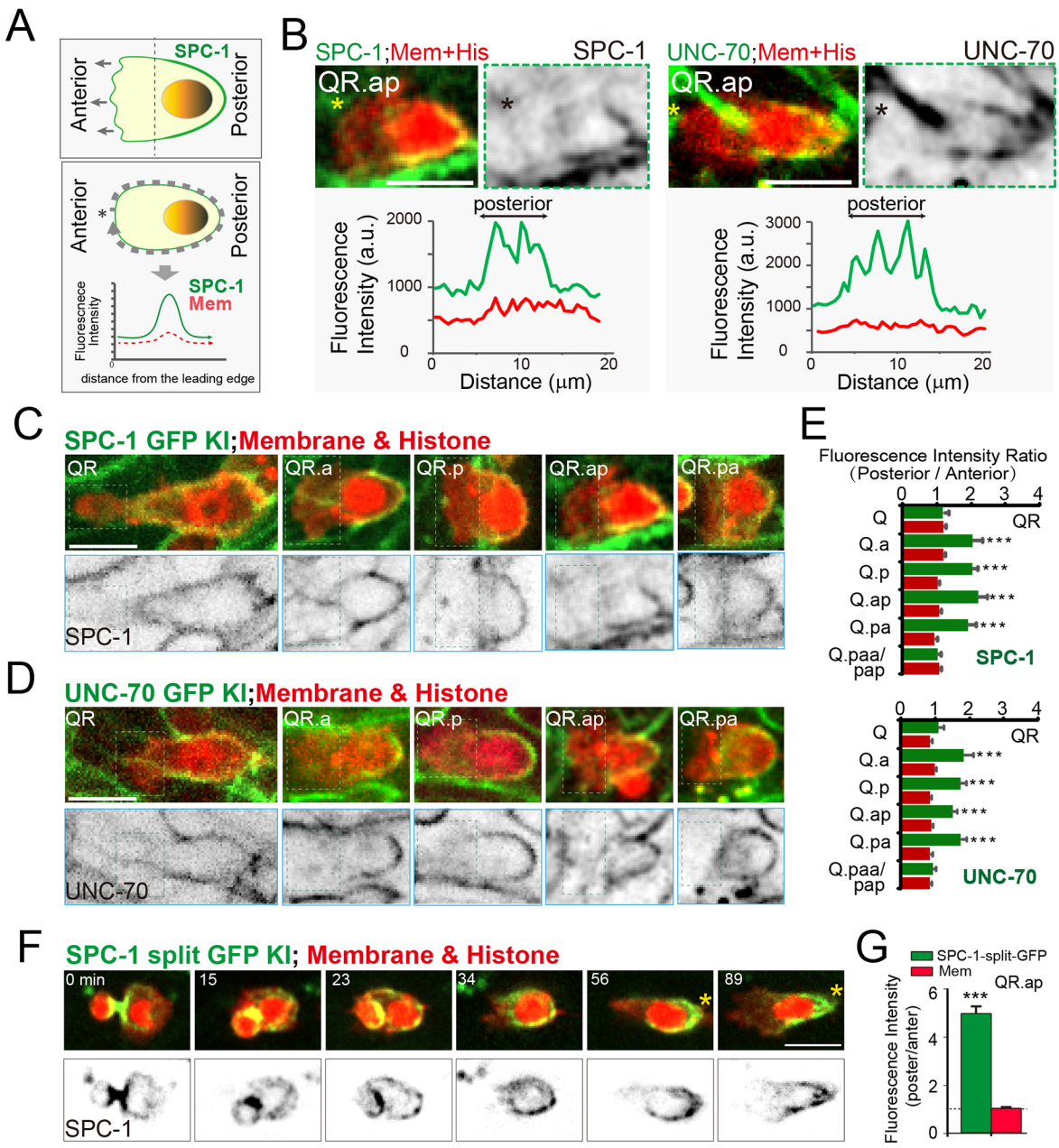

Fig. 2. SPC-1 and UNC-70 asymmetrically localize in the migrating cells. (A) Top: schematic of a migrating Q.x cell in SPC-1 GFP-knock-in *C. elegans*, showing GFP fluorescence enrichment at the rear portion of the migrating cell. Dashed line separates the anterior and posterior regions. Bottom: schematic showing quantification of GFP fluorescence intensity along the migrating cell periphery, starting from the leading spot, indicated with an asterisk, and proceeding along the dashed line around the Q.x cell. (B) Representative images of GFP-tagged SPC-1 (left) and UNC-70 (right) in QR.ap cells from knock-in animals. In each panel, upper left shows GFP KI fluorescence (green) with mCherry-tagged plasma membrane and histone (red), upper right shows inverted fluorescence images of GFP KI fluorescence, and the bottom panel shows the GFP (green) and mCherry (red) fluorescence distribution plot along the cell periphery of the representative image. Asterisk indicates the plot start point. (C,D) Fluorescence images showing, in green, GFP-tagged SPC-1 (C) or UNC-70 (D), and, in red, mCherry-tagged plasma membrane and histone in the QR lineage in KI animals. Lower panels show inverted images of the GFP-knock-in signal. A dashed box indicates the leading edge of each cell. (E) Quantification of GFP-tagged SPC-1 (top) or UNC-70 (bottom), and mCherry (red) fluorescence intensity ratio between the leading edge (indicated by dashed boxes in C,D) and the posterior plasma membrane in the QR cell lineages. Data are mean±s.e.m. of n=10–20 animals. See Fig. S1 for the QL lineage. (F) Fluorescence time-lapse images of split 7×GFP-tagged SPC-1, and mCherry-tagged plasma membrane and histone after QR.ap birth in WT. Top: merged images; bottom: inverted fluorescence signal of split 7×GFP-tagged SPC-1. Asterisk indicates the posterior of the cell. (G) Quantification of the fluorescence intensity ratio of 7×GFP-tagged SPC-1 (green), and mCherry-tagged membrane (red) between the posterior and the anterior of migrating QR.ap cells. Data are mean±s.e.m. of n=14 animals. Statistical significance is based on Student's t-test, ***P<0 0.001. Scale bars: 5 µm.

Fig. S1C). Spectrin was evenly distributed in Q neuroblasts, and in Q.paa and Q.pap cells, which do not undergo long-distance migration (Fig. 2E; Fig. S1C).

We sought to pinpoint how spectrin became asymmetrically localized in migrating Q cells. The GFP–spectrin KI strains illuminate spectrin in Q cells and their neighboring tissues, the high background fluorescence of which impedes the visualization of spectrin dynamics in Q cells. To resolve this problem, we adopted a self-complementing split fluorescent protein system (Jia et al., 2019; Kamiyama et al., 2016). We inserted seven copies of a

Journal of Cell Science (2020) 133, jcs248583. doi:10.1242/jcs.248583

GFP11 tag (7×GFP11), which encodes the eleventh β strand of super-folder GFP, into the *spc-1* locus and expressed GFP1–10 under the control of a Q cell-specific promoter, P*egl-17*. After genetically crossing an SPC-1::7×GFP11 knock-in animal with a P*egl-17*::GFP1–10 transgenic animal, GFP self-complemented and specifically illuminated spectrin with green fluorescence in Q cells. Using this strain, we confirmed that SPC-1::7×GFP fluorescence asymmetrically localized in the lateral region and the rear of migrating Q.ap cells, and found that the posterior enrichment of the localization was elevated from 2.7-fold in GFP knock-in animals to 5.2-fold in Q-cell specific SPC-1::7×GFP KI animals (Fig. 2G), possibly because of an increase of green fluorescence and elimination of background signal. Next, we followed the dynamic changes of spectrin during Q cell development. After Q cell division, spectrin accumulates at the cleavage furrow between two daughter cells (0 min, Fig. 2F; Movie 1). Spectrin then forms puncta outside of the front of the cell (23 min) and becomes enriched in the posterior (34–89 min), indicating an asymmetric assembly of the spectrin-based membrane skeleton in migrating cells (Fig. 2G; Fig. S1D).

The membrane skeleton remodels to safeguard dendrite formation

Our fluorescence time-lapse microscopy revealed that the timing and position of sprouting dendrites couples with cell migration. After the A/PQR neuron reaches its destination, the cell body stops, but the same leading-edge continues to elongate, transforming into the growth cone that forms the dendrite (Movie 2) (Li et al., 2017; Tian et al., 2015). We examined whether and how spectrin-based membrane mechanics regulate dendrite growth. In ∼10–30% of the *spc-1(cas971)* or *unc-70(cas983)* mutant animals, the A/PVM and A/PQR neurons developed neurites whose positioning and extent of growth were perturbed, and that were defective in formation, guidance or outgrowth (Fig. 3A–C). In WT animals, A/PVM neurons first extended their neurites in the dorsal/ventral (D/V) direction and then elongated along the anterior/posterior (A/P) body axis, and the PQR dendrite sprouted toward the posterior, with the axon growing toward the anterior. In the spectrin-deficient neurons, AVM improperly extended its axon to the posterior, the PVM axon skipped the initial D/V growth but underwent abnormal A/P growth, and PQR split its dendrite (red arrows in Fig. 3B).

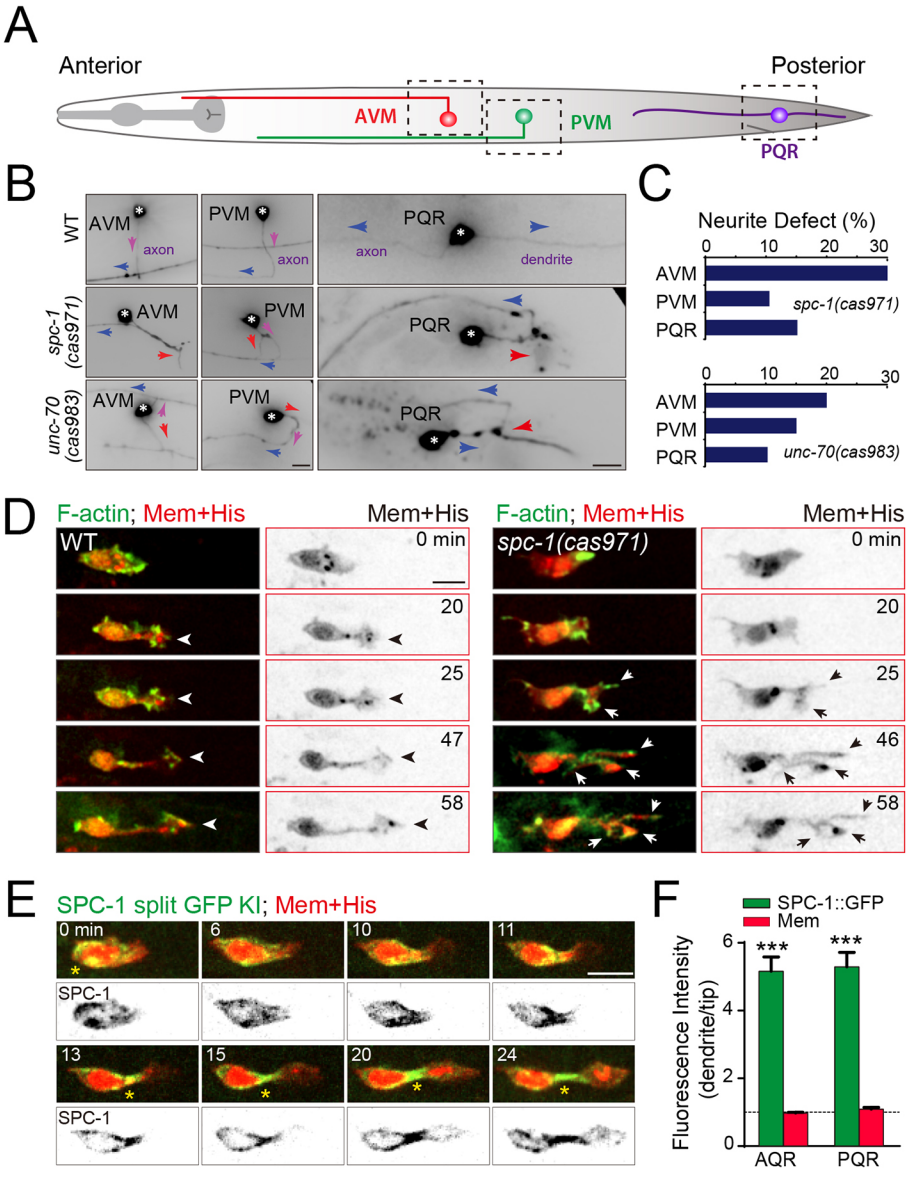

Fig. 3. SPC-1 regulates dendrite formation. (A) Schematic of the axon and dendrite morphologies of the Q-cell-derived neurons AVM, PVM, and PQR in WT animals. The regions shown in B are indicated by dashed boxes. (B) Neurites from AVM, PVM, and PQR neurons in WT, *spc-1(cas971)*, and *unc-70(cas983)* animals. The pink and blue arrows indicate the dorsal–ventral and anterior–posterior growth of the neurites, respectively, in WT animals, and the red arrows show misoriented neurites. Asterisk, cell body. Dendrites and axons were labeled and distinguished based upon information from wormatlas.org. (C) Quantification of defects in Q cell neuritogenesis in *spc-1(cas971)* (top) and *unc-70(cas983)* (bottom) mutant animals (*n*=60–100). (D) Fluorescence time-lapse images of GFP-labeled F-actin (green) and mCherry-tagged plasma membrane and histone (Mem+His, red) during QL.ap dendrite formation in WT and *spc-1(cas971)* mutant animals. In each panel, merged images are shown on the left, and inverted mCherry fluorescence images of cell morphology are shown on the right. Asterisk, nucleus; arrowhead, normal dendrite outgrowth direction towards the animal tail; arrow, misoriented dendrite in *spc-1(cas971)* mutant animals. (E) Fluorescence time-lapse images of 7×GFP-tagged SPC-1, and mCherry-tagged plasma membrane and histone during AQR neuritogenesis in WT. Top: merged images. Bottom: inverted fluorescence signal of split 7×GFP-tagged SPC-1. Asterisk indicates enrichment of 7×GFP-tagged SPC-1. (F) Quantification of the fluorescence intensity ratio of 7×GFP-tagged SPC-1 (green), and mCherry-membrane (red) between the new dendrite and growth cone of AQR and PQR cells. Data are mean±s.e.m. of *n*=10–14 animals. Statistical significance is based on Student's *t*-test, ***P<0.001. Scale bars: 50 µm (B), 5 µm (D,E).

Journal of Cell Science (2020) 133, jcs248583. doi:10.1242/jcs.248583

We performed live-imaging analysis of dendrite formation in PQR cells to address how spectrin regulates dendrite development. In WT animals, the PQR cell body arrived at the final destination, and the leading-edge continued to elongate, forming the growth cone for dendrite formation (Fig. 3D; Movie 2). F-actin accumulated at the leading edge, and the newly elongated dendrite became thin and stable (Fig. 3D). In spectrin mutants, the nascent dendrite was unstable and developed F-actin-enriched secondary growth cones that elongated and generated ectopic dendritic branches (Fig. 3D; Movie 3).

To understand spectrin behavior during dendrite formation, we followed SPC-1::7×GFP in the growing dendrite of the WT PQR neuron. SPC-1 initially accumulated in the lateral region and the rear of the migrating PQR; however, SPC-1 transited from the soma to the newly formed dendrite and became enriched in the dendrite (Fig. 3E). We did not detect SPC-1::7×GFP in the leading edge of the growth cone during dendrite outgrowth (Fig. 3E,F), which is consistent with the absence of spectrin in the leading edge of migrating cells. Quantification of the SPC-1::7×GFP ratio between the dendrite and the leading edge revealed a 5.3-fold enrichment (Fig. 3F). Taken together, these results show that the spectrin-based membrane skeleton disassembles in the soma and assembles in the nascent dendrite, where spectrin inhibits ectopic actin polymerization and safeguards dendrite morphology.

Ankyrin functions with spectrin during neural development

To dissect the molecular mechanism of how the spectrin-based membrane skeleton regulates neuronal cell migration and neurite growth, we used affinity purification and mass spectrometry to identify proteins that interact with SPC-1. Using an anti-GFP antibody, we purified GFP-tagged SPC-1 with its associated proteins from the lysate of SPC-1::GFP KI larvae (Fig. 4A). We determined protein constituents by using liquid chromatography–tandem mass spectrometry (LC-MS/MS) (Fig. 4B). We detected the β-spectrin subunit UNC-70, validating our purification scheme. Another top hit was UNC-44 (Table S4), an ortholog of the human ankyrin protein, which is another known binding partner of the membrane skeleton (Lorenzo, 2020). We have previously used the same GFP-affinity purification and mass spectrometry approach to identify binding partners for other proteins that are associated with the plasma membrane [e.g. MIG-13, a transmembrane protein essential for Q neuroblast migration (Zhu et al., 2016)]; however, we did not uncover UNC-70 and UNC-44, suggesting that the experimental pipeline can detect specific interactions. In *C. elegans*, UNC-44 regulates multiple neuronal events, including axon guidance, microtubule organization, and axon-dendrite sorting and transport (Maniar et al., 2011; Otsuka et al., 1995), but its functions in neuronal cell migration and dendrite development are less understood.

Using the *unc-44(e362)* allele or conditional *unc-44* mutants generated by somatic CRISPR-Cas9 (Fig. 4D), we showed that the loss of UNC-44 reduced Q cell migration in adult animals and disrupted the neurites in Q cell progenies, as observed for those in the spectrin mutant animals (Fig. 4H). By creating an UNC-44::GFP KI animal, we showed that UNC-44 was absent from the leading edge but accumulated in the lateral region and the rear of migrating Q cells (Fig. 4I,J; Movie 4), which is similar to the distribution of spectrin. We have previously reported the function of spectrin in ciliogenesis. In further support of the notion that UNC-44 acts with spectrin in the same processes, we found that the ciliary length and the capacity of the animal to interact with the environment (i.e. dye-filling) were defective upon the loss of UNC-44 (Fig. 4E–G). Using super-resolution live imaging, we showed that UNC-44 displayed periodicity in the axon of motor neurons (Fig. 4C). Double fluorescence imaging analysis revealed that the fluorescence intensity peaks from UNC-44::GFP and SPC-1::mCherry showed intercalation in the axon (Fig. 4C), which is consistent with the current model of the organization of the spectrin–ankyrin skeleton (Leterrier et al., 2017; Lorenzo, 2020; Xu et al., 2013). These results show that ankyrin functions together with spectrin in neuronal cell migration, the formation of the dendrite, and sensory cilia.

DISCUSSION

We provide evidence that the spectrin–ankyrin-based membrane skeleton is essential for neuronal cell migration and dendrite formation. This work reveals that the membrane skeleton is asymmetric and remodels during neural development. When neuroblasts migrate, spectrin accumulates in the lateral region and the rear of the cell; when neuroblasts use the same leading-edge to grow dendrites, spectrin transits from the soma to the nascent dendrites. In comparison to the polarized and dynamic actin and microtubule cytoskeleton, asymmetry and remodeling are not well appreciated for the membrane skeleton. Previous studies of spectrin used ‘snapshot’ imaging or fixed samples, and described the membrane skeleton as an immobile and stable structure underneath the entire plasma membrane (He et al., 2016; Leterrier et al., 2017; Lorenzo, 2020; Xu et al., 2013). In addition to its rigidity, asymmetry and remodeling can be essential for the function of the spectrin-based membrane skeleton. A polarized membrane skeleton can provide locally distinct membrane mechanics in a living cell (e.g. during cell migration), and the ability to remodel enables a developing cell to change its membrane mechanics at different developmental events (e.g. from cell migration to neurite outgrowth).

How can the spectrin-based membrane skeleton be asymmetric? Fluorescence microscopy of the cell from birth to migration revealed that the membrane skeleton becomes asymmetrically assembled in the posterior of the cell (Fig. 2F). The inhibition of spectrin localization in the leading edge might result from some unknown chemical cues. Alternatively, the space beneath the plasma membrane of the leading edge is occupied by the Arp2/3-nucleated branching actin cytoskeleton (Pollard and Cooper, 2009), the dense network of which might serve as a physical barrier to block assembly of the spectrin-based membrane skeleton. A similar physical inhibition might apply away from the front of the cell, where the membrane skeleton could prevent the recruitment of Arp2/3 and its activating protein machinery, blocking polymerization of the branched actin network in the lateral region and the rear of the cell.

Equally intriguing is how the assembled membrane skeleton is remodeled. Despite immense knowledge of the depolymerization of actin filaments and microtubules, little is known regarding the disassembly of the membrane skeleton. Signaling mediated by extracellular signal-regulated kinase (ERK) causes calpain-dependent degradation of the membrane-associated periodic structure, which suggests that activity of this kinase might be involved in remodeling of the membrane skeleton (Zhou et al., 2019). A protein kinase within the lateral region and rear of the migrating cell might phosphorylate spectrin and disassemble the membrane skeleton at the end of cell migration. Our previous study identified that the *C. elegans* Hippo kinases (CST-1 and CST-2) localize outside of the cell front and phosphorylate a small GTPase RhoG/MIG-2, inhibiting its Arp2/3-activating activity (Feng et al., 2017). Furthermore, a MAPK family kinase, MAP4K4,

Journal of Cell Science (2020) 133, jcs248583. doi:10.1242/jcs.248583

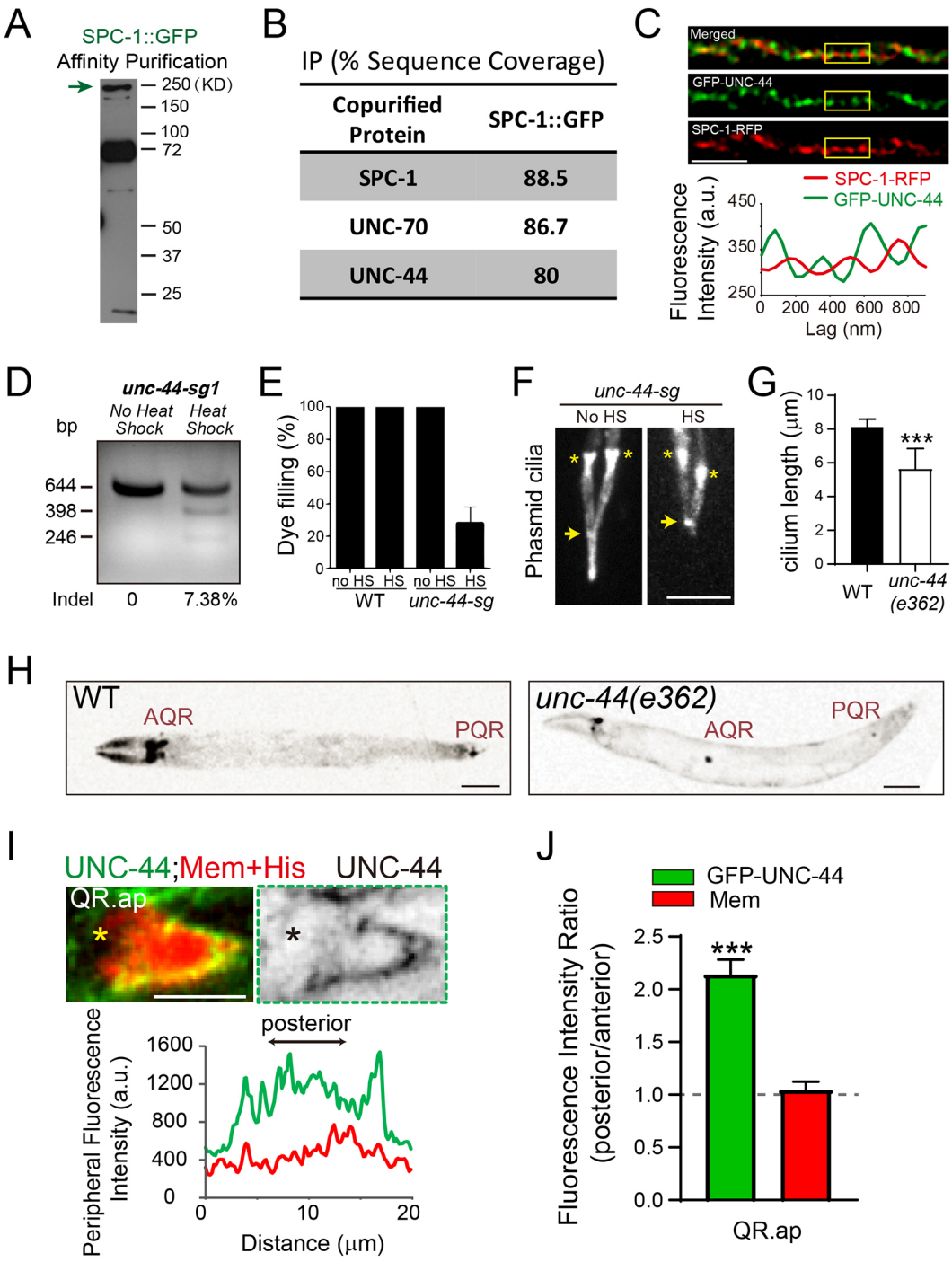

Fig. 4. See next page for legend.

phosphorylates the actin-membrane linker ERM in the rear of cells during mammalian cell migration (Vitorino et al., 2015). Such kinases might be involved in remodeling the membrane skeleton when the cell completes its movement. Alternatively, other kinases or other types of protein post-translational modifications might regulate disassembly of the membrane skeleton.

The spectrin-based membrane skeleton and the branched actin network appear to be mutually exclusive. The branched actin network assembled in the leading edge where spectrin is absent, and actin was ectopically assembled in the posterior of *spc-1*-deficient cells (Fig. 1F,G and Fig. 2C–G). Arp2/3-stimulated actin polymerization, coronin-based F-actin debranching, and ADF/cofilin-mediated F-actin severing empower a highly dynamic and protrusive membrane in the leading edge (Pollard and Cooper, 2009). The rigidity of the spectrin-based membrane skeleton offers stable membrane mechanics that maintain cell morphology of the migrating cells and the newly formed dendrite. The protrusive and rigid membrane domains in the same developing cell are thus well organized by the coordinated action of Arp2/3 and spectrin. Such a negative correlation between branched actin assembly and spectrin-based membrane mechanics provides insights into a long-standing question of how a migrating cell forms only one leading edge. A prevailing model posits that the plasma membrane tension constrains the spread of the leading edge and prevents the formation

Journal of Cell Science (2020) 133, jcs248583. doi:10.1242/jcs.248583

Fig. 4. UNC-44 interacts with SPC-1 and regulates neuroblast development. (A) Western blot with anti-GFP antibody showing the immunoprecipitation of SPC-1::GFP (indicated in the gel with the green arrow) from *C. elegans* using GFP-Trap beads. Size markers in kDa are indicated. (B) Mass spectrometry analysis of the SPC-1::GFP affinity purifications. The percentage sequence coverage is listed. (C) Representative images of GFP::UNC-44 (green) and SPC-1::RFP (red) in double knock-in animals (top, merged image; middle, GFP::UNC-44; bottom, SPC-1::RFP). The corresponding GFP::UNC-44 (green) and SPC-1::RFP (red) fluorescence intensity of the boxed region is shown below. Scale bar: 1 µm. (D) Representative gels of the T7EI assay for *unc-44* PCR products amplified from the genomic DNA of worms expressing P*hsp::Cas9* and P*U6::unc-44-sg1*, with or without heat-shock treatment. Percentage of DNA with insertion and deletion is indicated. (E) Dye-filling defects assayed under a fluorescence stereoscope (*n*>100 animals) of WT animals or worms expressing P*hsp::Cas9* and P*U6::unc-44-sg1*, with or without heat-shock (HS) treatment, respectively. (F) Cilium morphology in conditional *unc-44* mutants, with or without heat-shock treatment, visualized using an intraflagellar transport protein, IFT52/OSM-6::GFP. Arrows indicate the positions where the junctions between the middle and distal ciliary segments should be in WT animals. Asterisk, the ciliary base and transition zone. Scale bar: 5 µm. (G) Quantification of the cilium length from *n*=20 cells. (H) Inverted fluorescence images showing AQR and PQR position in WT and *unc-44(e362)* mutant animals. AQR and PQR neurons were visualized using P*gcy-32::mCherry*. The image is inverted so that high mCherry fluorescence intensity is black. Scale bars: 50 µm. (I) Representative images of GFP-tagged UNC-44 in QR.ap cells in knock-in animals, upper left shows GFP KI fluorescence (green) with mCherry-tagged plasma membrane and histone (red), upper right shows inverted fluorescence images of GFP KI fluorescence, and the bottom panel shows the GFP (green) and mCherry (red) fluorescence distribution plot along the cell periphery of the representative image shown above. Asterisk indicates the plot start point. Scale bar: 5 µm. (J) Quantification of the GFP (green)-tagged UNC-44 and mCherry (red) fluorescence intensity ratio between the posterior and the anterior membrane potions in migrating QR.ap cells (*n*=14 animals). Data in E,G,J are mean±s.e.m. Statistical significance is based on Student's *t*-test, ***P<0.001.

of new fronts. For example, migrating neutrophils use plasma membrane tension as a physical inhibitor to impede actin assembly outside of the existing front (Houk et al., 2012), but the molecular basis of such physical tension is unclear. The spectrin-based membrane skeleton might play a previously unrecognized, yet potentially widespread, role in membrane tension during different types of cell migration.

SPC-1 and UNC-70 are subunits of the spectrin complex, and mutations of both proteins similarly reduced neuronal migration (Fig. 1B) and disrupted dendrite outgrowth (Fig. 3B,C), leading to uncoordinated animal behavior. These data suggest that SPC-1 and UNC-70 might play a similar function during neuronal development. Our findings that the hereditary elliptocytosis-associated α-spectrin mutation and the spinocerebellar ataxia type 5-associated β-III-spectrin deletion resulted in defective in neuronal cell migration and neurite formation support the notion that spectrin-based membrane mechanics plays multiple roles in neural development, providing additional insights into SCA5 pathogenesis. Our results will motivate future investigations to examine whether neuronal migration or axon and dendrite formation are abnormal in Purkinje cells and granule cell progenitors with hereditary elliptocytosis or spinocerebellar ataxia. The manipulation of mechanobiology in the nervous system might merit exploration as a potential therapeutic strategy for some types of neurodegenerative disorders.

MATERIALS AND METHODS

C. elegans strains and genetics

C. elegans strains were raised on NGM plates (3 g NaCl, 17 g Bacto-agar, 2.5 g Bacto-peptone, 1 ml cholesterol, 1 ml of 1 M CaCl, 1 ml of 1 M $MgSO_4$, and 25 ml of 1M KPO_4, pH 6, per liter in dH_2O) seeded with *E. coli* strain OP50 at 20°C. Tables S1–S3 summarize the primers, plasmids, and strains used in this study.

Molecular biology

CRISPR-Cas9 targets were inserted to the pDD162 vector (Addgene #47549) by linearizing this vector using the primers listed in Table S1. The resulting PCR products containing 15 bp overlapped double-strand DNA ends were digested with DpnI overnight and transformed into *E. coli*. The linearized PCR products were cyclized to generate plasmids through spontaneous recombination in bacteria. For fluorescence tag knock-ins, homologous recombination (HR) templates were constructed by cloning the 2 kb 5′ and 3′ homology arms into the pPD95.77 plasmid (Addgene; www.addgene.org) using an In-Fusion Advantage PCR cloning kit (Clontech, cat. no. 639621). We used the CRISPR design tool (http://crispr.mit.edu) to select the target sequence. GFP, 7×GFP11, and RFP tags were added to the C-terminus of SPC-1, whereas UNC-70 and UNC-44 were tagged with an N-terminal GFP. We generated SPC-1-L268P and UNC-70-ΔH590-L598 mutation knock-ins in the SPC-1::GFP and GFP::UNC-70 knock-in background using similar cloning strategies. Conditional knockout strains were generated and determined as previously described (Shen et al., 2014).

Microinjection and transgenesis

For SPC-1 split GFP knock-in generation, P*egl-17*::GFP1–10 constructs were generated by cloning *egl-17* promotor and GFP1–10 sequences into pPD95.77 plasmids using an In-Fusion Advantage PCR cloning kit (Clontech, cat. no. 639621). The plasmid was injected into SPC-1::7×GFP11 knock-in animals. Transgenic strains were generated by microinjecting ∼50 ng/µl DNA with co-injection markers into *C. elegans* germlines.

Mass spectrometry analysis

Unsynchronized SPC-1::GFP knock-in strains raised on ∼80–100 90-mm NGM plates were collected and washed three times with M9 buffer (5.8 g Na_2HPO_4, 3.0 g KH_2PO_4, 0.5 g NaCl, 1.0 g NH_4Cl per liter in dH_2O). Lysates were made from ∼1–2 ml packed worms in lysis buffer [25 mM Tris-HCl, pH 7.4, 150 mM NaCl, 1% NP-40, 10% glycerol, 1× protease inhibitor cocktail (Complete EDTA free, Roche), 40 mM NaF and 5 mM Na_3VO_4] and ∼3–4 ml of 0.5-mm diameter glass beads using a FastPrep-24 homogenizer (MP Biomedicals). Proteins were immunoprecipitated using GFP-Trap A beads (Chromoteck) and eluted with 300 ml 0.1 M glycine-HCl, pH 2.5 into 15 ml 1.5 M Tris-HCl, pH 8.8, followed by precipitation with 100 ml trichloroacetic acid. Samples were redissolved in 60 ml 8 M urea and 100 mM Tris-HCl, pH 8.5. Samples were treated with 5 mM TCEP for reduction, 10 mM iodoacetamide for alkylation, and then diluted fourfold with 100 mM Tris-HCl pH 8.5. The proteins were digested with 0.2 mg trypsin at 37°C overnight, after the addition of 1 mM $CaCl_2$, and 20 mM methylamine. The resultant peptides were desalted using Zip Tip pipette tips (Merck Millipore). The tandem mass spectrometry spectra were searched against the *C. elegans* proteome database using Proteome Discoverer (version PD1.4; Thermo Fisher Scientific). The protein components in the list in Fig. 4 were reproducibly identified from three biological repeats.

Dye-filling assay

Young-adult worms were randomly collected into 200 µl M9 solution and mixed with equal volume of dye (DiI stain; 1,1′-Dioctadecyl-3,3,3′,3′,-tetramethylindocarbocyanine Perchlorate; Sigma-Aldrich, St Louis, MO, USA) at working concentration (20 µg/ml), followed by incubation at room temperature in the dark for 30 min. Worms were transferred to seeded NGM plates and examined for dye uptake 1 h later using a fluorescence stereoscope. At least 100 worms of each strain were examined in two independent assays.

Live-cell imaging

Q cell migration imaging was performed using a previously described protocol (Zhu et al., 2016). L1-stage worms were anesthetized using 0.1 mmol/l levamisole in M9 buffer and mounted on 3% agarose pads at

20°C, then imaged on an Axio Observer Z1 microscope (Carl Zeiss) equipped with a 100×, 1.49 numerical aperture (NA) objective, an electron-multiplying (EM) charge-coupled device (CCD) camera (Andor iXon+ DU-897D-C00-#BV-500), and the 488 nm and 561 nm lines of a Sapphire CW CDRH USB Laser System attached to a spinning disk confocal scan head (Yokogawa CSU-X1 Spinning Disk Unit). Time-lapse images were acquired using µManager (https://www.micro-manager.org) at an exposure time of 200 ms. Images of spectrin and UNC-44 periodicity with 150 nm *x-y* resolution were collected on a Nikon (Tokyo, Japan) A1R laser-scanning confocal microscope using a CFI Plan Apo 100× oil immersion objective (NA 1.45) and 488-nm lasers.

Quantifications and statistical analysis

ImageJ software was used to circumscribe the fluorescence field and to measure the fluorescence intensity. In all the intensity quantifications, the background was subtracted. When the F-actin marker GFP::moesinABD or knock-in fluorescent protein signal intensity was measured along the cortex, 'leading' refers to the circumference of the lamellipodium (the widespread area) and 'rear' refers to the circumference around the rest of the cell body, and the intensity ratio between the two was calculated using the corresponding mCherry fluorescence intensity as a control. Migration distances were measured as the cell body movement (in µm/h) along the anterior–posterior body axis. The migration angle was measured between the cell protrusion and the anterior–posterior body axis. The anterior was defined as 0°, and the posterior was defined as 180°. Quantifications were represented as the mean±s.d. for each group. N represents the number of animals used for the corresponding quantification, and a one-sample or two-tailed Student's *t*-test or χ^2 analysis were employed to determine statistical differences, as indicated in figure legends.

Competing interests

The authors declare no competing or financial interests.

Author contributions

Conceptualization: G.O.; Methodology: C.X.; Investigation: R.J.; Resources: R.J., G.L., Z.Z.; Data curation: Y.C.; Supervision: K.H., W.L., G.O.; Project administration: G.O.; Funding acquisition: G.O.

Funding

This work was supported by the National Key R&D Program of China (2017YFA0503501, 2019YFA0508401, and 2017YFA0102900) and the National Natural Science Foundation of China (grants 31730052, 31525015, 31561130153, 31671444 and 31871352).

Supplementary information

Supplementary information available online at https://jcs.biologists.org/lookup/doi/10.1242/jcs.248583.supplemental

Peer review history

The peer review history is available online at https://jcs.biologists.org/lookup/doi/10.1242/jcs.248583.reviewer-comments.pdf

References

Feng, G., Zhu, Z., Li, W. J., Lin, Q., Chai, Y., Dong, M. Q. and Ou, G. (2017). Hippo kinases maintain polarity during directional cell migration in Caenorhabditis elegans. *EMBO J.* **36**, 334-345. doi:10.15252/embj.201695734

Gaetani, M., Mootien, S., Harper, S., Gallagher, P. G. and Speicher, D. W. (2008). Structural and functional effects of hereditary hemolytic anemia-associated point mutations in the alpha spectrin tetramer site. *Blood* **111**, 5712-5720. doi:10.1182/blood-2007-11-122457

Hammarlund, M., Davis, W. S. and Jorgensen, E. M. (2000). Mutations in beta-spectrin disrupt axon outgrowth and sarcomere structure. *J. Cell Biol.* **149**, 931-942. doi:10.1083/jcb.149.4.931

Han, B., Zhou, R., Xia, C. and Zhuang, X. (2017). Structural organization of the actin-spectrin-based membrane skeleton in dendrites and soma of neurons. *Proc. Natl. Acad. Sci. USA* **114**, E6678-E6685. doi:10.1073/pnas.1705043114

Harper, S. L., Sriswasdi, S., Tang, H.-Y., Gaetani, M., Gallagher, P. G. and Speicher, D. W. (2013). The common hereditary elliptocytosis-associated alpha-spectrin L260P mutation perturbs erythrocyte membranes by stabilizing spectrin in the closed dimer conformation. *Blood* **122**, 3045-3053. doi:10.1182/blood-2013-02-487702

He, J., Zhou, R., Wu, Z., Carrasco, M. A., Kurshan, P. T., Farley, J. E., Simon, D. J., Wang, G., Han, B., Hao, J. et al. (2016). Prevalent presence of periodic actin-spectrin-based membrane skeleton in a broad range of neuronal cell types and animal species. *Proc. Natl. Acad. Sci. USA* **113**, 6029-6034. doi:10.1073/pnas.1605707113

Houk, A. R., Jilkine, A., Mejean, C. O., Boltyanskiy, R., Dufresne, E. R., Angenent, S. B., Altschuler, S. J., Wu, L. F. and Weiner, O. D. (2012). Membrane tension maintains cell polarity by confining signals to the leading edge during neutrophil migration. *Cell* **148**, 175-188. doi:10.1016/j.cell.2011.10.050

Ikeda, Y., Dick, K. A., Weatherspoon, M. R., Gincel, D., Armbrust, K. R., Dalton, J. C., Stevanin, G., Dürr, A., Zühlke, C., Burk, K. et al. (2006). Spectrin mutations cause spinocerebellar ataxia type 5. *Nat. Genet.* **38**, 184-190. doi:10.1038/ng1728

Jia, R., Li, D., Li, M., Chai, Y., Liu, Y., Xie, Z., Shao, W., Xie, C., Li, L., Huang, X. et al. (2019). Spectrin-based membrane skeleton supports ciliogenesis. *PLoS Biol.* **17**, e3000369. doi:10.1371/journal.pbio.3000369

Kamiyama, D., Sekine, S., Barsi-Rhyne, B., Hu, J., Chen, B. H., Gilbert, L. A., Ishikawa, H., Leonetti, M. D., Marshall, W. F., Weissman, J. S. et al. (2016). Versatile protein tagging in cells with split fluorescent protein. *Nat. Commun.* **7**, 11046. doi:10.1038/ncomms11046

Leterrier, C., Dubey, P. and Roy, S. (2017). The nano-architecture of the axonal cytoskeleton. *Nat. Rev. Neurosci.* **18**, 713-726. doi:10.1038/nrn.2017.129

Li, W., Yi, P., Zhu, Z., Zhang, X., Li, W. and Ou, G. (2017). Centriole translocation and degeneration during ciliogenesis in Caenorhabditis elegans neurons. *EMBO J.* **36**, 2553-2566. doi:10.15252/embj.201796883

Liem, R. K. (2016). Cytoskeletal integrators: the spectrin superfamily. *Cold Spring Harb. Perspect Biol.* **8**, a018259. doi:10.1101/cshperspect.a018259

Lorenzo, D. N. (2020). Cargo hold and delivery: Ankyrins, spectrins, and their functional patterning of neurons. *Cytoskeleton (Hoboken)* **77**, 129-148. doi:10.1002/cm.21602

Lorenzo, D. N., Badea, A., Zhou, R., Mohler, P. J., Zhuang, X. and Bennett, V. (2019). betaII-spectrin promotes mouse brain connectivity through stabilizing axonal plasma membranes and enabling axonal organelle transport. *Proc. Natl. Acad. Sci. USA* **116**, 15686-15695. doi:10.1073/pnas.1820649116

Maniar, T. A., Kaplan, M., Wang, G. J., Shen, K., Wei, L., Shaw, J. E., Koushika, S. P. and Bargmann, C. I. (2011). UNC-33 (CRMP) and ankyrin organize microtubules and localize kinesin to polarize axon-dendrite sorting. *Nat. Neurosci.* **15**, 48-56. doi:10.1038/nn.2970

Norman, K. R. and Moerman, D. G. (2002). α spectrin is essential for morphogenesis and body wall muscle formation in Caenorhabditis elegans. *J. Cell Biol.* **157**, 665-677. doi:10.1083/jcb.200111051

Otsuka, A. J., Franco, R., Yang, B., Shim, K. H., Tang, L. Z., Zhang, Y. Y., Boontrakulpoontawee, P., Jeyaprakash, A., Hedgecock, E., Wheaton, V. I. et al. (1995). An ankyrin-related gene (unc-44) is necessary for proper axonal guidance in Caenorhabditis elegans. *J. Cell Biol.* **129**, 1081-1092. doi:10.1083/jcb.129.4.1081

Ou, G. and Vale, R. D. (2009). Molecular signatures of cell migration in C. elegans Q neuroblasts. *J. Cell Biol.* **185**, 77-85. doi:10.1083/jcb.200812077

Pollard, T. D. and Cooper, J. A. (2009). Actin, a central player in cell shape and movement. *Science* **326**, 1208-1212. doi:10.1126/science.1175862

Ranum, L. P. W., Schut, L. J., Lundgren, J. K., Orr, H. T. and Livingston, D. M. (1994). Spinocerebellar ataxia type 5 in a family descended from the grandparents of President Lincoln maps to chromosome 11. *Nat. Genet.* **8**, 280-284. doi:10.1038/ng1194-280

Shen, Z., Zhang, X., Chai, Y., Zhu, Z., Yi, P., Feng, G., Li, W. and Ou, G. (2014). Conditional knockouts generated by engineered CRISPR-Cas9 endonuclease reveal the roles of coronin in C. elegans neural development. *Dev. Cell* **30**, 625-636. doi:10.1016/j.devcel.2014.07.017

Sulston, J. E. and Horvitz, H. R. (1977). Post-embryonic cell lineages of the nematode, Caenorhabditis elegans. *Dev. Biol.* **56**, 110-156. doi:10.1016/0012-1606(77)90158-0

Tang, N. H. and Jin, Y. (2018). Shaping neurodevelopment: distinct contributions of cytoskeletal proteins. *Curr. Opin. Neurobiol.* **51**, 111-118. doi:10.1016/j.conb.2018.02.022

Tian, D., Diao, M., Jiang, Y., Sun, L., Zhang, Y., Chen, Z., Huang, S. and Ou, G. (2015). Anillin regulates neuronal migration and neurite growth by linking RhoG to the actin cytoskeleton. *Curr. Biol.* **25**, 1135-1145. doi:10.1016/j.cub.2015.02.072

Vitorino, P., Yeung, S., Crow, A., Bakke, J., Smyczek, T., West, K., McNamara, E., Eastham-Anderson, J., Gould, S., Harris, S. F. et al. (2015). MAP4K4 regulates integrin-FERM binding to control endothelial cell motility. *Nature* **519**, 425-430. doi:10.1038/nature14323

Wang, G., Simon, D. J., Wu, Z., Belsky, D. M., Heller, E., O'Rourke, M. K., Hertz, N. T., Molina, H., Zhong, G., Tessier-Lavigne, M. et al. (2019). Structural plasticity of actin-spectrin membrane skeleton and functional role of actin and spectrin in axon degeneration. *Elife* **8**, e38730. doi:10.7554/eLife.38730.041

Wang, X., Zhou, F., Lv, S., Yi, P., Zhu, Z., Yang, Y., Feng, G., Li, W. and Ou, G. (2013). Transmembrane protein MIG-13 links the Wnt signaling and Hox genes to the cell polarity in neuronal migration. *Proc. Natl. Acad. Sci. USA* **110**, 11175-11180. doi:10.1073/pnas.1301849110

Xu, K., Zhong, G. and Zhuang, X. (2013). Actin, spectrin, and associated proteins form a periodic cytoskeletal structure in axons. *Science* **339**, 452-456. doi:10.1126/science.1232251

Zhou, R., Han, B., Xia, C. and Zhuang, X. (2019). Membrane-associated periodic skeleton is a signaling platform for RTK transactivation in neurons. *Science* **365**, 929-934. doi:10.1126/science.aaw5937

Zhu, Z., Chai, Y., Jiang, Y., Li, W., Hu, H., Li, W., Wu, J.-W., Wang, Z. X., Huang, S. and Ou, G. (2016). Functional coordination of WAVE and WASP in C. elegans neuroblast migration. *Dev. Cell* **39**, 224-238. doi:10.1016/j.devcel.2016.09.029